In-orbit performances of the EIT instrument on-board SOHO and intercalibration with the EIT Calroc Sounding rocket program

Jean Marc Defise[a],
John Daniel Moses[b], Frédéric Clette[c],
and the EIT Consortium*

[a]Centre Spatial de Liège, Avenue Pré-Aily, B-4031 Angleur, Belgium, jmdefise@ulg.ac.be
[b]Naval Research Laboratory, Washington, DC 20375
[c]Observatoire Royal de Belgique, Avenue Circulaire, B-1180 Bruxelles, Belgium

ABSTRACT

The Extreme UV Imaging Telescope (EIT) instrument is operating on-board the SOHO spacecraft since January 1996. EIT is providing EUV observations of the solar corona in four narrow channels: 171, 195, 284 and 304 Å.
Due to continuous exposure to the EUV solar irradiation, the instrument performance is continuously evolving. The backside thinned detector is showing important changes in its overall response and local damages of EUV highly exposed areas. These performance modifications can be characterized through several observation analyses that are discussed in this paper. Two major effects are identified: contamination on the detector surface and charge mobility changes in the CCD produced by the EUV irradiation. To restore the instrument response, bakeouts are regularly planned as well as specific observation sequences that are used to characterize the detector damages. An overview of the instrument response behavior is presented in this paper.
To cross calibrate this instrument, the spare components of the EIT program were assembled in a new structure used as the EIT Calroc Sounding Rocket instrument. The Calroc flight successfully occurred in October 97 and gathered very useful data that provide additional means to cross calibrate the EIT-SOHO instrument. The Calroc results and their use to improve the EIT-SOHO data are discussed. This sounding rocket mission demonstrated good correlations of the performance monitoring analyses on the EIT-SOHO with the diagnostic deduced from the Calroc observations.

Keywords: EUV solar corona, EUV CCD, radiation aging, contamination.

1. INTRODUCTION

The EIT (Extreme UV Imaging Telescope) instrument is part of the SOHO payload, launched on December 2, 1995 and orbiting around the L1 Lagrangian point since February 96. Permanently pointed towards the Sun, EIT [1] is imaging the solar corona in four narrow EUV bandpasses defined by multilayer coatings deposited on normal incidence optics: 171, 195, 284 and 304 Å. At the focal plane of the telescope, a 1024 x 1024 pixel CCD is detecting the solar radiation. This detector was specially processed for EUV sensitivity enhancement. Each collecting element has a 2.6 x 2.6 arcsec viewing angle over the solar corona observed from the SOHO spacecraft. The instrument underwent a ground-based calibration program that provided a complete calibration of the system [2], in order to fulfill all the scientific objectives of the instrument.
Since the first months of operations, that started in early 1996, the instrument has been operating nominally. However, the response of the instrument has been evolving and changing from the initial laboratory measurements [3]. Important modifications in both the global response and the local sensitivities were recorded. Therefore, it was essential to maintain an up-to-date characterization of the overall sensitivity of the CCD, as well as relative sensitivities of all the individual pixels (flat fielding). Specific studies were then carried out to characterize the in-flight response during the mission period, to

* Information on the EIT Consortium and the EIT instrument is available at http://umbra.nascom.nasa.gov/eit.

preserve the scientific quality of the EIT extensive synoptic observation program. Some results of these studies are discussed in this paper.
In parallel with the first operations of the EIT instrument, the EIT-CALROC sounding rocket program was being built with all the spare parts of the initial EIT-SOHO project. A very similar instrument has been assembled in a rocket structure. Extensive on-ground tests were conducted before the CALROC flight, to gather flatfields, bandpasses and CCD performances. The CALROC mission was successfully flown in October 97, 22 months after the start of the EIT-SOHO mission. The main objectives of the mission were to produce a complete set of EUV solar observations in the 4 channels, simultaneously with the EIT-SOHO instrument. Despite the short duration of the sounding rocket flight, essential data were gathered with the CALROC observations. We will discuss the comparison of the simultaneous observations, as well as the main results that can be extracted from them.

2. EVOLUTION OF THE EIT RESPONSE ON-BOARD SOHO

2.1 Introduction

EIT has been continuously observing the EUV Sun in a constant environment due to the extremely stable attitude of the SOHO platform, continuously pointing towards the Sun in the L1 orbit. The EIT instrument is operated continuously to provide a global survey of the rising phase of the solar cycle, that will reach its next maximum near 2001. The CCD detector is permanently cooled down to -67°C with a passive radiator viewing the cold space, while the rest of the telescope is thermally controlled at +20°C. During the first two years of operations, more than 67,000 EUV images were gathered with the instrument.
Since its first light in January 1996, the instrument throughput showed important variability [4,5], that can be unambiguously distinguished from the solar variability. The four EUV channels are affected by these sensitivity modifications, with different levels of degradation. Changes have also been detected in the visible light response of the detector, using the on-board calibration lamps.
The detector is a 1024 x 1024 pixel back-thinned CCD equipped with a decontamination heater, that was used initially to outgas the condensed material from its cooled collecting surface. Bakeout sequences are periodically planned, increasing the CCD temperature to about +15°C. These sequences affect directly the CCD response, which requires an accurate characterization. Each CCD bakeout produces an immediate but partial recovery of the response.
There is evidence that degradation of the detector occurs where high EUV irradiation reaches the CCD. As most of imaging EUV detectors currently available for spaceflight applications, the EIT detector is subject to damage by EUV exposure. We will show that this loss of sensitivity can be partly annealed during the bakeouts. These response changes can be discussed based on several detection techniques. The observed variations are discussed in section 2.2 to 2.4, and the proposed explanations are discussed in section 2.5.

2.2 The overall response of the instrument

The main trends in the sensor response are illustrated by the plots of the total response evolution during the first two years of operations shown in figure 1. The bakeout sequences are identified by vertical lines. These plots provide the average degradation, assuming the solar EUV flux is constant. They are built from the total signal of each full field image. The instrument is imaging the EUV emission at 4 wavelengths, ranging from 171 to 304 Å. This type of analysis provides useful information only in these two extreme wavelengths. The total signal of the other two central bandpasses is corrupted by the solar variability and the longitude distribution of the solar features at 195 and 284 Å. The 171 Å is also affected in a lower extent by the quasi-periodic passage of solar active regions in the field of view.

The total response in the visible can be evaluated using the calibration lamp mode. These incandescent lamps illuminate the detector diffusely with visible and near-infrared light, providing images that can be used to monitor the evolution of the detector response in this wavelength range. Included also in figure 1, the total detector response to calibration lamp exposure has been plotted versus the mission date. Long operating periods at -67°C obviously produce a loss of detector response.

These diagnostics provide only information on the total response of the sensor. They do not allow to tell the difference between global and local losses of sensitivity that are present in the EUV and the visible.

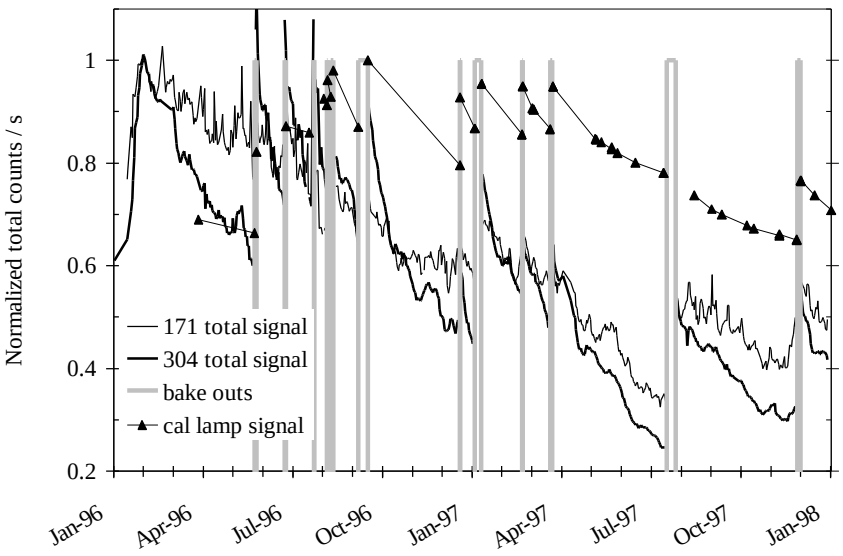

Figure 1: The EIT total response in the two EIT bandpasses (171 and 304 Å) covering the range of all four observed wavelengths. These plots are median filtered over 24 hour intervals.
Also included in this figure is the total response obtained in the visible with the calibration lamp. Vertical lines indicate the bakeout periods.

From figure 1, we can also point out the similar trends of the visible channel with the EUV ones, i.e. an overall decrease interrupted by bakeouts that partly restore the throughput. The 304 Å channel exhibits the largest response changes.

2.3 Local burned-in features

After an unexpectedly long overexposure when the shutter was left accidentally open for several hours in July 96 in the 304 Å channel, it became clear that high EUV exposure can damage the internal structure of the detector. In normal operation, several regions of the field of view are always more exposed to the EUV irradiation: the solar limb, the disk, 2 east-west belts where the active regions are crossing the field in the northern and southern hemispheres of the solar disk, and an inverted grid pattern produced by the filter supporting grid. Due to the very stable pointing of SOHO, that keeps the EUV sun always in the center of the EIT field of view, damages to the detector sensitivity accumulate in those areas.

In order to quantify the EUV damage, we have investigated the grid pattern degradation which is the only absolutely fixed brightness structure in the field of all the EUV images. In the close vicinity of the focal plane, a focal aluminium filter is intercepting the EUV converging beam. This filter is made of a thin (1500 Å) aluminium foil supported by a nickel mesh used to improve the mechanical properties of the assembly. The occultation produced by the mesh in direct proximity with the detector results in a regular pattern in all the EIT images. It can be shown theoretically that this pattern is mainly a result from a shading effect of the 40 µm thick rods in the 440 µm period square mesh, located at about 15 mm in front of the focal plane.
Due to the off-axis position of the four different (non circular) entrance pupils of the four EIT passband channels, the resulting modulation pattern of the focal plane filter support is different for each observed wavelength. The four grid signatures are slightly shifted spatially, as well as symmetrically reversed. In all the cases, the shadow of the focal filter mesh results in a periodic modulation grid pattern superimposed on the EUV sun images. The grid pattern is visually apparent mainly on the solar disk area and just above the limb, where the photon flux is highest. Specific techniques were developed to extract the grid modulation from the EIT images, based on the first months of data and using the very regular pattern of the nickel mesh [3]. They provide solar images free of grid shading effect.
After several months of operations, a new dark grid pattern began to appear on all the images, mainly in the detector area covering the solar disk region. The variability of the EUV solar disk made this faint dark pattern quite difficult to identify. However, after the first burn in incident, the effect of EUV illumination was clearly identified. The new dark grid imprint can also be attributed to the effect of the steady modulation pattern of the local EUV irradiation. The focal filter always produces the same inverted burned-in pattern on same areas for each given bandpass. Therefore, in the long run, this

permanent modulated illumination imposed a modulation of the damage to the CCD response, producing a dark pattern corresponding to a weighted contribution of the four grid signatures.
The calibration lamp images also provide useful additional information on the detector response in visible light degradation. This dark grid pattern can also be identified (Fig. 13) in the sensitivity degradation.

Intercorrelation analyses were conducted to identify the burned-in imprint. Due to the high level noise in the dark pattern, this method can only identify the location of the highest peak in the intercorrelation functions computed between the four grid patterns. The 304 Å grid is the one producing a centered maximum in the intercorrelation function, demonstrating that over the first two years of EIT operations, the 304 Å observations are mainly responsible for the CCD response degradation.

Another approach has been developed in order to evaluate the respective damaging effects of the four separate wavebands imaged by EIT. It provides also a way to quantify the recovery rate of the imprint after each bakeout sequence. The idea is to measure the contrast of the dark imprint. A first selection is applied on four different sets of highlighted regions corresponding to the mesh crossings in the four original grid shadow patterns within the solar disk area.
Figure 2 shows one of the grid signatures, with the contour of the highlighted regions to be considered. It is then possible to evaluate the **local** ratios of the signal in these regions by the signal in regions taken in local adjacent mesh centers (dark regions of figure 2). For each grid cell, a set of a dozen of points is used to evaluate the corresponding ratios. Analyzing the median of the overall sets of ratios in the solar disk region (8,000 sampled points), we can derive a figure that characterizes the EUV damage potentially produced by the original grid signature. This technique has the advantage to avoid any dependency to the local bright features that appear in the solar images, as it is based on images rotationally averaged over several hours and on the median value of the ratios.

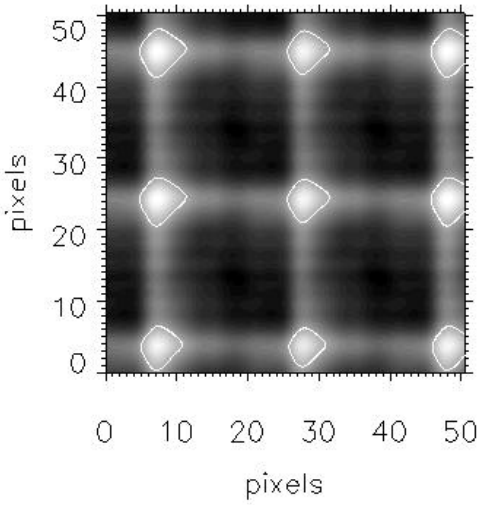

Figure 2: Highlighted areas in one of the grid signatures

Figure 3 shows a plot of the temporal evolution of the median ratio on 304 Å average images. From these plots, that were normalized to March 1, 1996 data, we can infer that the 304 Å and the 195 Å observations are producing most of the dark grid features, as their ratios are decreasing at a higher rate.

This figure demonstrates also that the bakeout sequences (vertical lines) have a direct annealing effect that produces partial suppression of the dark grid imprint within the dark solar disk region. The global signal recovery has no influence on this diagnostic, giving evidence that EUV damage can be restored by baking out. One by-product of this analysis is to provide a clear diagnostic on the local damages due to high EUV cumulated dose. It provides a way to evaluate the effect of the bake-outs on those damaged regions.

Shown in figure 4, the comparison of the response damage by the 304 Å grid in the 171 and the 304 Å channels confirms the general response trend of figure 1: the 304 Å channel is the most affected by the EUV damage.

A similar analysis was also conducted on single calibration lamp images, providing information on the visible response of the detector. The dark grid contrast evolution is shown in figure 5. The 304 Å observations appear also clearly as the main source of damage. The long term trend is more stable than what is obtained in the EUV. This figure confirms that the visible response is also affected by EUV exposure, and not only by the deposit of a uniform condensed layer that should produce only a very small loss of signal in that wavelength range. The bakeout effect is also beneficial in terms of grid imprint suppression, giving also evidence that annealing occurs in the silicon wafer.
However, the damage rate as well as the absolute sensitivity loss are fairly different in the visible and the EUV.

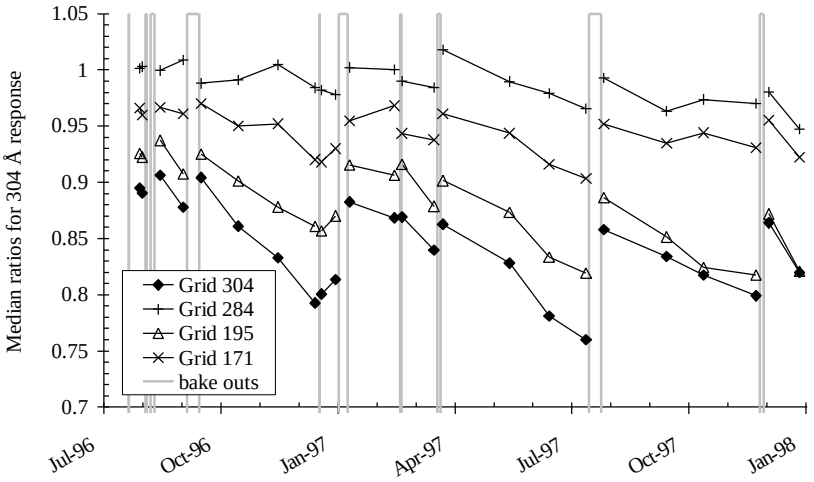

Figure 3: Grid imprint damage in the 304 Å images obtained with the median ratios of the signal in high and low modulated regions for each grid signature (see text). Low ratios indicate high contrast and high damage. Dates and durations of the bakeout sequences are shown with vertical lines.

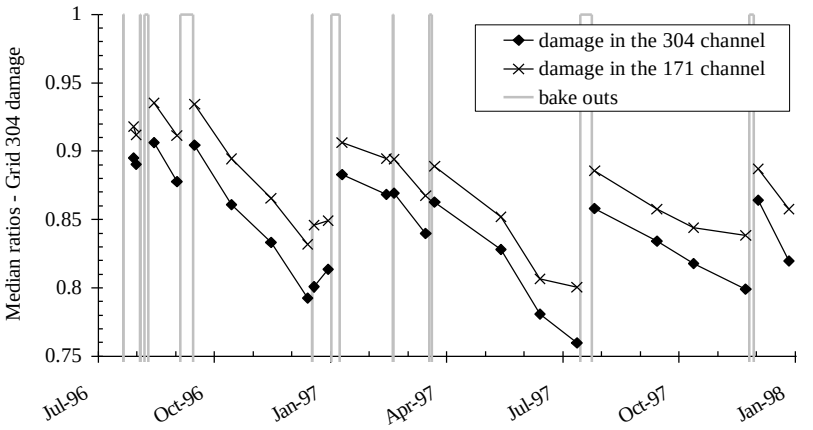

Figure 4: Comparison of the 304 grid damage in the 304 and the 171 Å channels. These plots are the median ratios of the high to the low signal regions of the 304 grid modulation, in the 171 Å and 304 Å response. This shows that the damage is more important in the 304 channel (lower ratios and higher contrast).

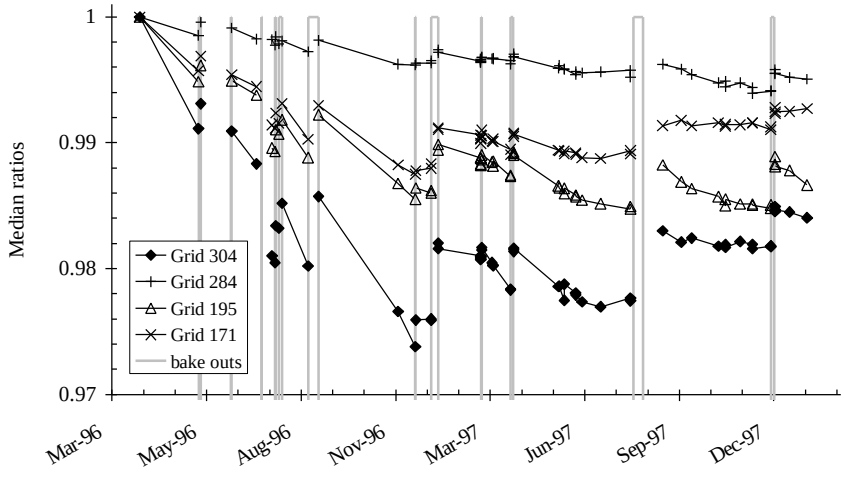

Figure 5: Evolution of the dark grid imprint in the visible response of the EIT detector. The low ratios correspond to higher contrast and higher response damage

These degradations can be correlated with the EUV dose received on each individual pixel during the first two years of the mission. A survey of all the images taken by the instrument has been run. Interpolations of full field images were included in the survey to cover the subframe modes. This heavy analysis provided maps of the total signal per pixel for every day of the mission. Using these maps, it was possible to build plots (Fig. 6) of the grid imprint contrast in the 304 images versus the cumulated dose of each EIT channel inside the disk. In figure 6, it appears that there is a direct relationship between the total dose and the EUV degradation. The bakeouts are easy to identify in this plot by the sharp decreases in the damage contrast, although the percentage decrease is not consistent from bakeout to bakeout, or wavelength to wavelength. This analysis has relevant limitations due to the response damages that affect the total signal maps.

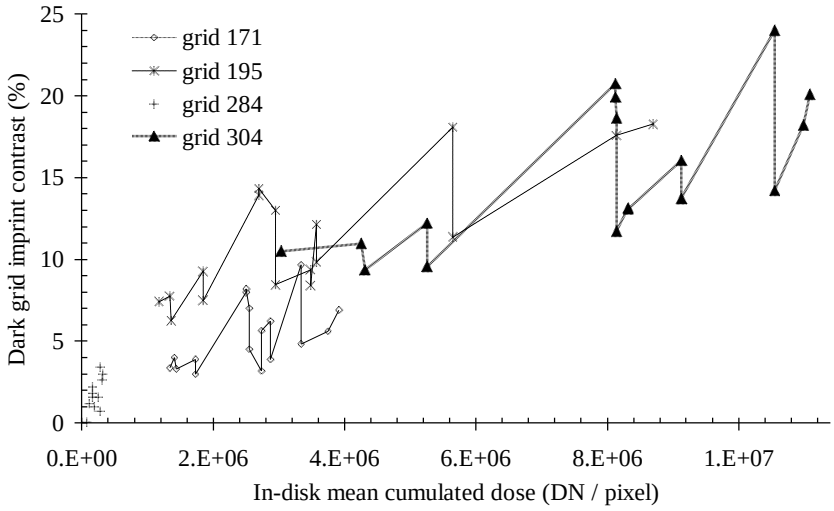

Figure 6: Dark grid imprint function of the in-disk cumulated dose. Vertical lines refer to bakeouts that provide grid imprint reduction.

These analyses are very useful to provide some understanding of the degradation process and to define least destructive operating modes of the instrument.

2.4 Additional inflight diagnostic methods

A program dedicated to the CCD health monitoring has been defined and is run periodically. Several techniques are employed: the visible light response with calibration lamp images, the dark current of the detector, the response linearity in the EUV and a survey of local burned-in regions. These sequences are also run systematically just before and after each CCD bakeout to allow direct evaluation of the restoration.

- Using photon transfer analyses [6], it was demonstrated that the EUV damage can affect the CCD charge collection efficiency (CCE) [4]. The important burned-in blemish that occurred end of Jul-96 (shown in figure 7.a) has been monitored in this way, and after 15 months (figure 7.b), this local blemish has been annealed and is now undistinguishable from the local background that also suffered from high EUV exposure. The survey was performed with periodic high-cadence subframe images, used to extract the shot noise function of the signal. This method presents several limitations, due to the limited read out speed combined with solar variability and due to assumptions in the analysis. Figure 7.c relates the evolution of the photon/DN parameter in this blemish after 15 months elapsed after the incident. For this evaluation, the PT analysis was conducted over 15x15 pixel regions sliding along the X axis of figure 7.a. The resulting photon/DN parameter (sliding average over 15x15 pixels) is shown in figure 7.c, giving evidence that the blemished area was affected by a CCE decrease (05-Aug-96 plot of fig. 7.c). These figures also indicate that 15 months of operations led to a general decay of the on-disk sensitivity.

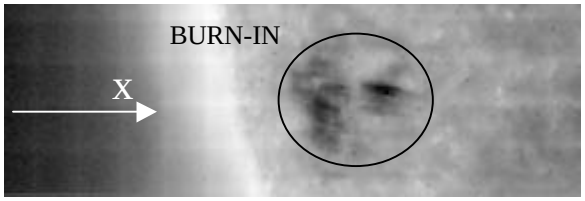

Figure 7.a: Burned-in area in early Aug-96 (171 Å, 288 x 96 pixels).

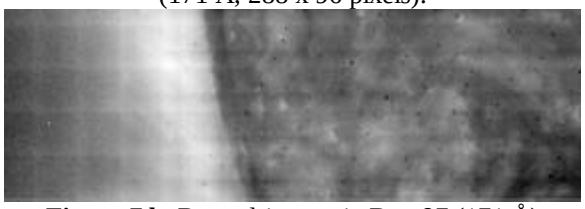

Figure 7.b: Burned-in area in Dec-97 (171 Å)

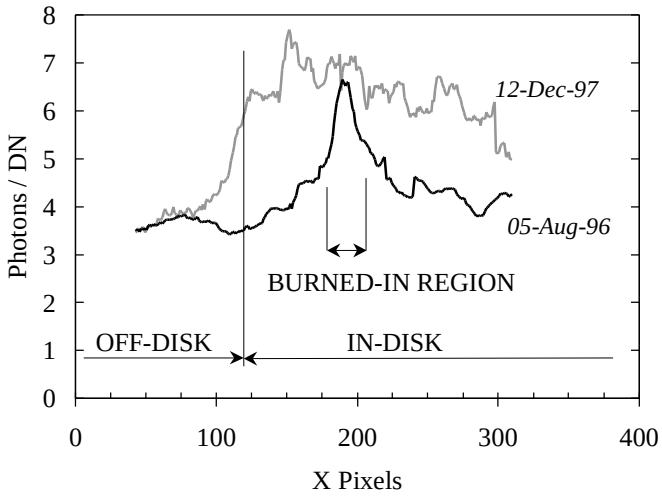

Figure 7.c: PT analyses results at 171 Å

- Dark images are regularly taken to determine the dark current of the detector. No significant change is found at the -67°C operating temperature, as shown in figure 8, with the survey of the dark counts recorded during the readout time (total = 20 s). However, this monitoring program demonstrated that extended operating periods are affecting the dark counts in the "solar disk" area of the chip when heated to room temperature. Again, bakeout sequences have a direct annealing effect on the traps and defects contributing to this dark current.

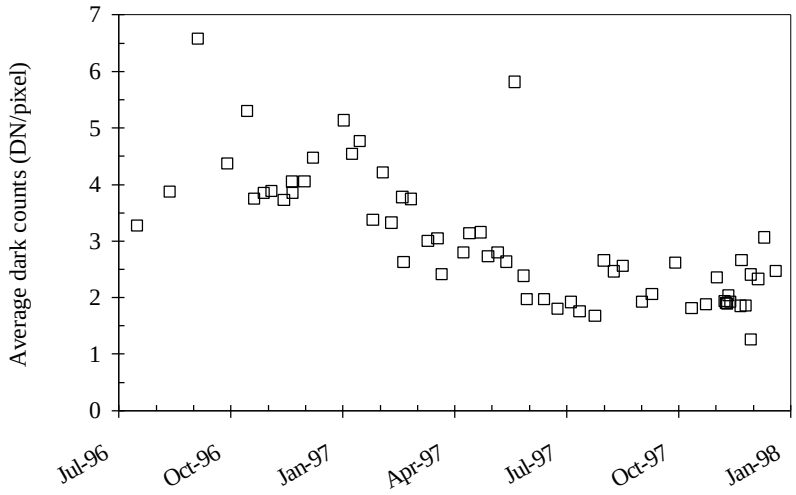

Figure 8: Average dark counts at -67°C over the first two years of the mission (0 s exposure time + 20 s readout time). The dark counts in operating conditions remain very acceptable, knowing that full well capacity corresponds to 2^{14} DN.

At higher temperature, dark current is significantly enhanced in the solar disk region. Again, bakeout sequences provide partial restoration of the dark current uniformity over the whole detector, and reduce the current itself. Figure 10 shows the ratio of two dark images taken before and after the Jul-97 bakeout at +2°C during the read out time, in 2x2 binned mode. White regions correspond to important dark current reduction after CCD warming. On figure 9, we display the histogram of the dark images in the in-disk region, where the dark counts are higher. The improvement shown in figure 9 and 10 is detailed in table 1. In-disk and off-disk dark counts are respectively reduced to 30% and 40 % of their initial value. The standard deviation change indicates improvement of the uniformity.

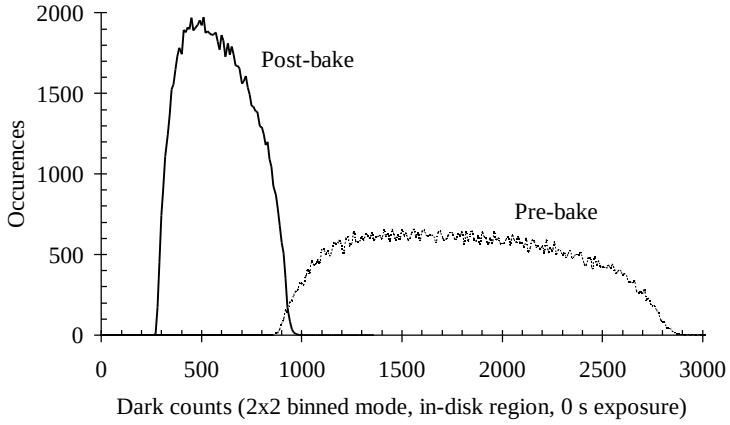

Figure 9: Histograms of dark current at T=+2°C in pre-bakeout and post-bakeout images

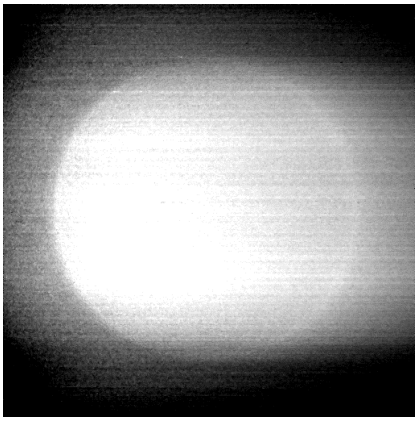

Figure 10: Ratio of pre to post-bakeout dark current images at T=+2°C

CCD warming Jul-97 T=+2°C	In disk average DN/4 pixels	Off disk average DN/4 pixels	Standard deviation DN/4 pixels
Pre bake	1816	1264	743
Post bake	588	459	245

Table 1: Dark current improvement with CCD bakeout

- The survey of the calibration lamp signal leads to other insights on the aging evolution. In addition to the global variation of the visible throughput discussed in section 2.2, the calibration lamp images show a darkening in the disk region (Fig. 13), that reflects a local decrease of the visible response. In order to quantify the on-disk damage, we made a survey of the visible signal in regions inside and outside the disk. The good stability of the lamp illumination can be used to compare the resulting images before and after bakeouts. The results of this survey are illustrated in figure 11 with the ratio of the on-disk to the off-disk mean signal per pixel. The ratios are normalized to the ratio of the calibration lamp image of May 1996. The step increases in the ratio plot of figure 11 indicate preferential recovery in the disk region with the bakeouts. The continuous decreases show the visible response damage in the detector area covered by the EUV solar disk relative to the off-disk region with the cumulated EUV exposures, that again reveals damage increase in the response of high EUV exposed detector pixels.

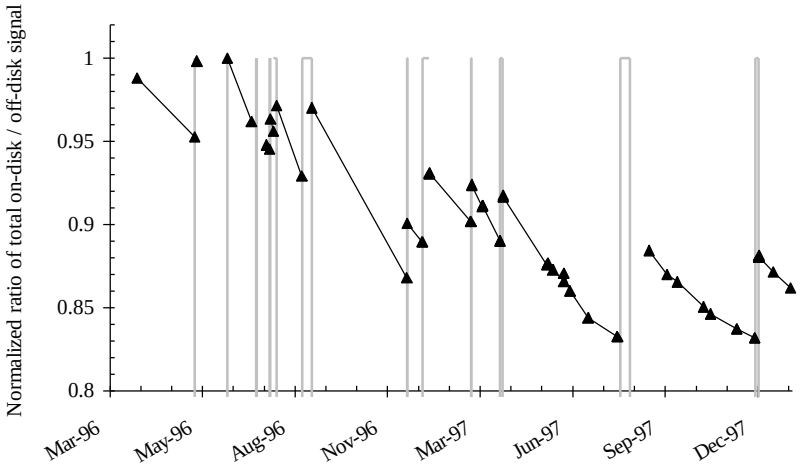

Figure 11: Ratio of the on-disk mean signal to the off-disk mean signal in the visible calibration lamp images, with normalization to the May-96 ratio.

2.5 Aging processes affecting the EIT throughput

Several parameters are affecting the response of the EIT instrument, making the interpretation of the aging process difficult.

The main results of the response monitoring program can be summarized as:

- the whole surface of the detector is affected by a response change in both EUV and visible channels
- high EUV irradiation reaching the detector affects the local response in both EUV and visible channels
- high EUV irradiation is degrading the EUV CCE
- EUV degradation is more important in the EUV than in the visible
- EUV degradation is more important at 304 Å than in the 3 other EUV channels
- dark current at high temperature is increased where the detector is exposed to high EUV irradiation
- detector bakeouts have an immediate (but partial) effect on the overall EUV and visible response
- dark current at high temperature is reduced and partly uniformized with bakeouts

From these primarily results, several diagnostics can be established.

The changes that affect uniformly all the detector pixels in the beginning of the mission can be attributed to the effect of condensed material on the cold surface of the detector. The smaller level of degradation in the visible confirms this diagnostic, as the EUV photons are more easily absorbed by potential contaminants. This condensed material may originate from the remaining gas left in the instrument before launch, or from outgassing of internal components, despite the efforts to launch the instrument with internal vacuum and the stringent cleanliness program followed during the construction of the instrument. The very first part of the EIT mission (figure 1, January to February 96) shows an overall throughput increase, that can be explained by the general outgassing of the filters and optical surfaces once exposed to the space environment. This period is then followed by the accumulation of condensed material in the detector cavity, that has a very small vacuum conductance. The rapid overall response restoration is the result of the evaporation process during temperature cycling.

The local response damages corresponding to high EUV irradiated regions could result from an EUV-induced opacification of the condensed material on the detector surface. In this case, the bakeouts would not lead to response recovery in the solar disk. Therefore, if this effect is involved, it only slightly contributes to these local degradations. On the other hand, CCE degradation was identified as the main contributor to the sensitivity loss in EUV damaged areas. This CCE decrease can result from modifications of the external silicon oxide layer of the detector. The behavior of this kind of back-thinned CCD is known to be very sensitive to the configuration of the oxide layer [7]. A possible mechanism would be the electrical charging of the native SiO_2 oxide and the generation of interface trap sites. The high EUV illumination can produce radiation-induced holes in the oxide, causing a shallow potential well for electrons, or capturing electrons from the silicon lattice. These two effects (charge trapping and interface states) are known to be the main consequences of total dose radiation. The overall instrument throughput showed an important acceleration of the degradation starting in March 1996 (figure 1), corresponding to the start of the global solar EUV survey observing program, which increased the EUV exposure. This is then the beginning of the EUV degradations in the detector. The dark current rise at warm temperature and its annealing also give important information on the presence of interface states.

The dark features in the calibration lamp images corresponding to the EUV blemishes indicate that CCE may also be reduced in this wavelength range, and that contamination is not the only damaging factor for these images.

All these studies indicate that two main processes are taking part to the EUV response decrease: condensed material on the cold collecting surface of the CCD and CCE degradation. These two processes affect the four EUV channels of the instrument differently. The penetration depth of the 304 Å photons is the smallest among the three other EUV bandpasses. Therefore, the 304 Å channel showing the deepest response changes indicates that the degradation mechanisms occur at the vicinity of the CCD front surface. This behavior is consistent with the types of degradation processes that have been identified.

3. THE EIT-CALROC PROGRAM

The objective of the EIT-CALROC program* is to increase the scientific return from the EIT-SOHO spaceflight mission with well calibrated supporting observations using the flight spare EIT-SOHO elements on a sounding rocket platform. Improvement of the absolute calibration of the EIT-SOHO observations is needed because of limitations in pre-flight calibrations imposed by the SOHO instrument integration schedule, and the complex variations in the EIT EUV response observed in-flight. Since the observed EUV response variations are a wavelength dependent combination of uniform and local effects in the SOHO EIT images, only a full disk imaging instrument is capable of providing an adequate calibration.

Therefore, joint efforts were carried out to build a second EIT instrument adapted to a rocket flight. Spare optics, spare detectors and spare mechanisms were assembled and qualified in a new structure. A ground-based calibration has been performed to identify and characterize the photometric and spectral responses of the new instrument. The final preparation took place in 1997, and was concluded by a successful launch on October 16, 1997 from the White Sands Missile Range (NM). In spite of a 5 minute observing schedule, the EIT-CALROC provided a complete set of observations [7] in all the channels, at the apogee of the flight, at 350 km altitude, corresponding to the minimum absorption of the residual atmosphere. Simultaneously with the rocket flight, the EIT on-board SOHO recorded similar data from the L1 Lagrangian point, located at 1,500,000 km from earth.
Despite a slight decentring of the pointing, an additional electronic noise perturbation and a small light leak in the 284 channel, the CALROC data provide a unique opportunity to build detailed and accurate primary calibration maps of the EIT-SOHO sensor after 22 months of in situ operations. The payload was retrieved after the launch in good condition for post-flight calibration that will eventually confirm the pre-flight data.

4. EIT-SOHO DIAGNOSTIC WITH EIT-CALROC DATA

4.1 The EIT-CALROC calibration maps

The EIT-CALROC was operated in a 2X2 binned mode, producing then 512 x 512 pixel images in order to save integration and readout time during the short duration of the mission. On board SOHO, EIT was also operated in the same mode, to allow fast cadence and to increase chances of exposure overlaps with CALROC in each channel.
After preparation of the EIT-CALROC data, it was possible to compute a "pixel to pixel" ratio map (in 2X2 binned mode) between both sets of observations. This technique leads directly to flat-field maps of the EIT-SOHO instrument, valid for October 16, 1997.

The calibration maps are shown in figures 12, where the dark regions correspond to the reduced EIT-SOHO response. The noise seen in the corners of the ratio maps is mainly due to an electronic noise, while sharp, small-scale solar structures are artifacts due to the time difference between the SOHO and CALROC images (rotational shifts). The CALROC light leak at 284 Å produces a defect that is detectable in the lower left part of the corresponding figure 12.c.
A first analysis of these figures confirms the results of previous studies. The limb darkening, the two dark belts on the disk, the overall disk and the grid imprint are the areas where the relative sensitivity is degraded. Other features within the disk are identical in all the maps, meaning that they form part of the calibration map.

For all the channels, the disk region shows a mean degradation of 75 % relative to the off-disk region, while the relative response decrease reaches 85 % in the limb, corresponding to the darkest regions of figures 12.

* Additional information about the Calroc program is available at http://lasco-www.nrl.navy.mil/calroc.html.

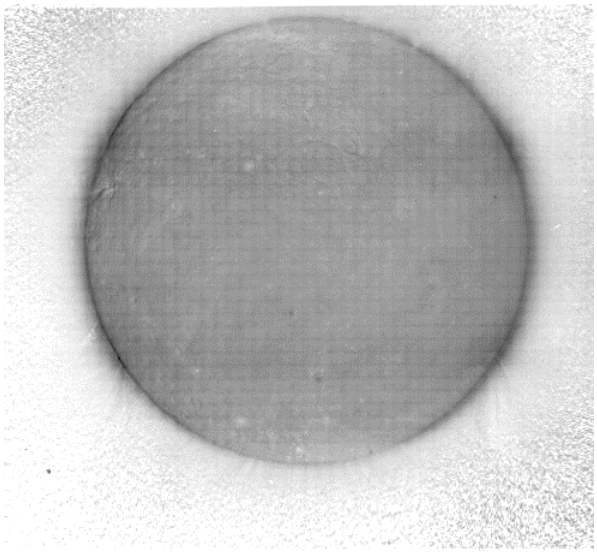

Figure 12.a: Calibration map at 171 Å

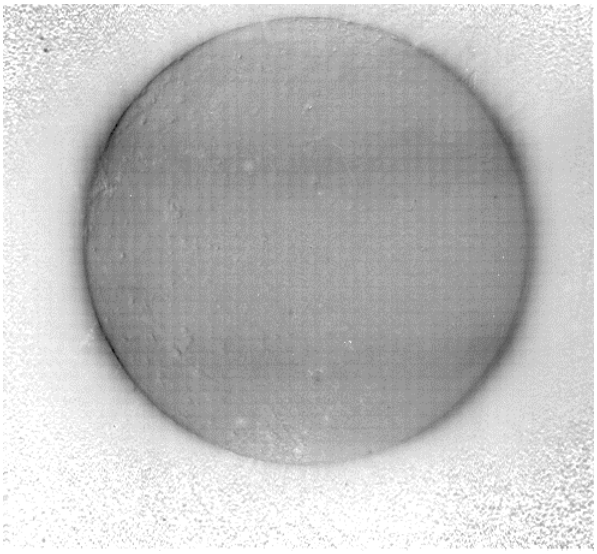

Figure 12.b: Calibration map at 195 Å

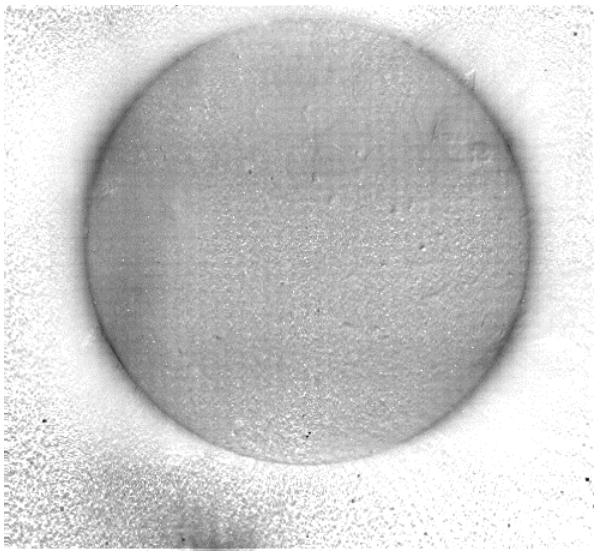

Figure 12.c: Calibration map at 284 Å

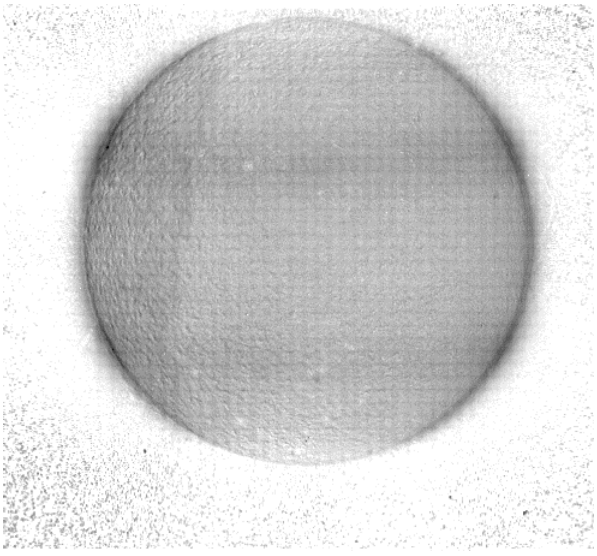

Figure 12.d: Calibration map at 304 Å

4.2 Assessment of the previous studies

The EIT-CALROC calibration maps can be compared to the ratio of the calibration lamp signal on October 16, 1997 with the first calibration lamp image, i.e. March 96 serving as "undegraded" reference. This gives a map of the response evolution since almost the start of the mission in the visible range.

Comparing this ratio map with the figures 12, we find a very good agreement. The limb, the disk and grid blemishes are common to figure 12 maps and figure 13. There are also other lighter regions on the disk, that are now confirmed to be genuine in-flight detector blemishes.

As had already been detected before the CALROC flight, the amplitude of the degradation is lower in the visible [4]. For example, the loss of sensitivity in the disk darkening is only of 15 % at visible wavelength, while it reaches 80 % in the EUV.

However, given the agreement between these results, we can thus infer that calibration lamps can be a precious tool to implement time-varying corrections to the EUV data during the mission period.

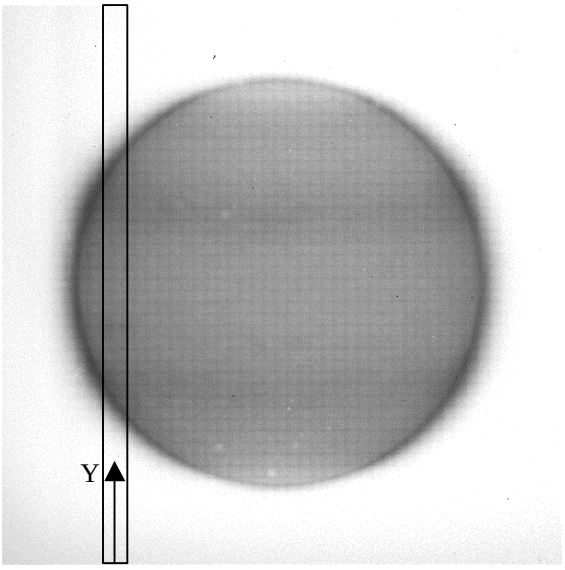

Figure 13: Ratio of Mar-96 to 16-Oct-97 SOHO-EIT calibration lamp images.

The photon transfer (PT) analysis [6] was applied to the in-flight data to evaluate the amount of signal loss and to confirm that the radiation damages affect the CCE of the CCD. The results of this technique applied on in-flight data [4] have been confirmed with a PT analysis based on a sequence of mid Oct-97. A fast cadence sequence at 171 Å was run on the region defined by the vertical subframe area (32 pixels wide) of figure 13, using a specific shutterless mode to improve the speed of the readout process and reduce the changes of the solar flux between each frame. This area includes the off-disk, 2 limb regions, and an in-disk region. The PT analysis over sliding subframes of 32 x 5 pixels gives the photon / DN parameter along the Y axis, which is directly related to the CCE. The comparison of these results with the CALROC calibration data over the same region is shown in figure 14.

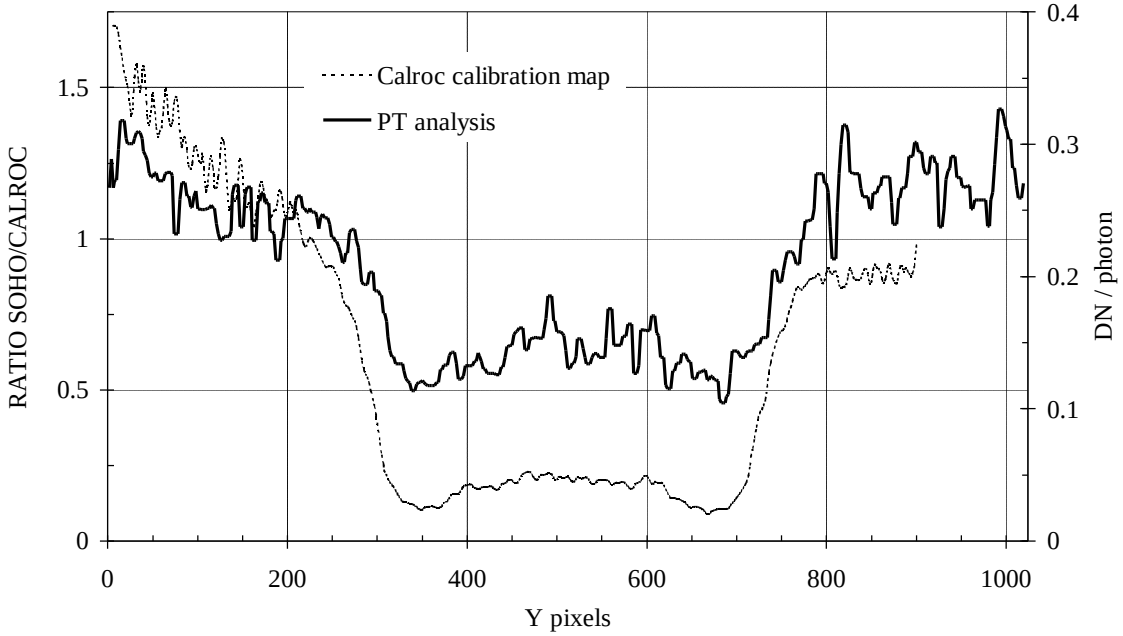

Figure 14: Comparison of the PT result (DN/photon) and the Calroc calibration map over a 32 pixel wide subframe of figure 13.

The PT analysis gives confirmation that the limb and the disk darkening are mainly resulting from CCE degradation. Although this technique has limitations when used with solar images, it provides unique informations about the CCD intrinsic damages. However, CCE decrease alone cannot account for the total difference of degradation levels observed inside and outside the limb.

The degradation with the total dose can also be analyzed with the Calroc calibration maps. The map of the total dose received on each individual pixel at the date of October 16, 1997 is also affected by the CCD response changes. A very rough correction for the cumulated dose in each wavelength can be estimated with an average of the Calroc to SOHO ratio with a damage-free map. Applying this corrected total dose map for each EIT channel, one can compute the individual pixel response change as a function of the local cumulated dose. This development has some limitations, due to the rough assumption of the average correction that does not take into account bakeout effects as well as variable damage rate and distribution during the mission time. The result of this computation is illustrated in figure 15, showing the response changes in each wavelength with the cumulated total dose in all the EUV bandpass channels. This plot is obtained after median filtering of data subsets.

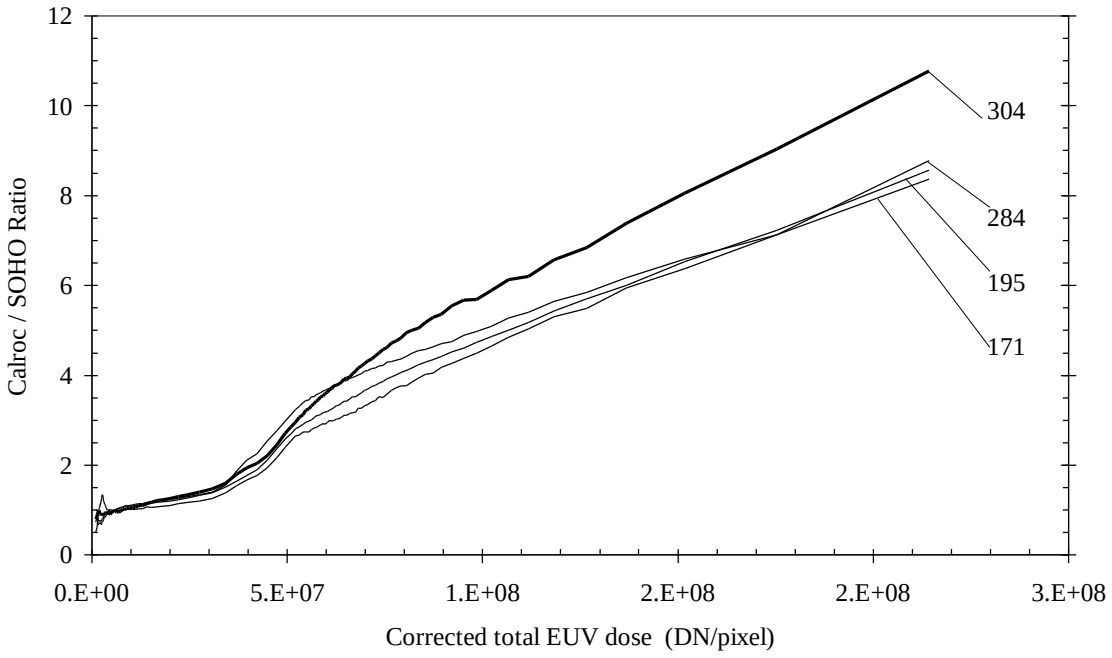

Figure 15: The Calroc to SOHO ratio in each channel function of the cumulated dose in each individual pixel, at the date of October 16, 1997.

The direct relationship between the damage and the EUV dose is confirmed. For high cumulated dose, each channel has a linear trend, with a slope increasing with the wavelength. This gives an additional clue to the superficial nature of the damage in the CCD wafer, that affects more the 304 Å photons with their smaller penetration depth.

5. CONCLUSIONS

The EIT-SOHO mission is a complete success in terms of scientific return after the first two years of operations. The good health of the instrument is promising excellent results until the completion of the mission, scheduled after the year 2000. This success will be enhanced with the achievement of the post calibration work that should provide aging corrections for all the EIT data.

The response changes are clearly identified, and can now be quantified by a set of diagnostics that are discussed in this paper. The EIT-Calroc mission confirms the results of the in-flight calibration analyses. The Calroc calibration maps provide a unique reference for the flat field corrections. Based on this and on other calibration analyses, one should be able

to derive updates of these maps for any mission day, and to identify the relative amounts of degradation produced by CCE decrease and accumulation of condensed material on the detector. A new flight of the EIT-Calroc experiment will be scheduled in the forthcoming months to upgrade once more the corrections.

These studies on the response aging have a direct impact on the operational management of the EIT instrument. Understanding now that the 304 Å observations are the most damaging among the 4 EIT bandpasses motivated new policies in the EIT operating modes. Due to the solar structure of the He II emitting ions, one single 304 Å image collects more photons over all the solar disk than the other wavelengths. On the other hand, the currently ongoing high cadence coronal mass ejection of the 195 Å channel is also increasing the total dose on the detector, bringing the 195 Å channel to a similar damaging effect than the 304 Å.

The partial response restoration provided by bakeout sequences generates difficulties in recalibrating the data with the Calroc references. As shown in this paper, the post-bakeout signal improvement is not the same for all the damaging processes, inducing variations in the Calroc maps. On the other hand, bakeouts provide direct response improvement, that may avoid permanent detector damages. Therefore, bakeouts are only planned after long observation periods or crucial high cadence imaging series.

6. ACKNOWLEDGMENTS

The EIT-SOHO and the EIT-CALROC programs are developed with support from NASA (NDPRS-86759E and NDPRS-09930F), US Office of Naval Research, Belgian OSTC and French CNES. We wish to thank the EIT Operation Team for their support to this intercalibration work.

7. REFERENCES

1. Delaboudinière et al, "EIT: Extreme-UV imaging telescope for the SOHO mission", Solar Physics **162**, 291-312, 1995.
2. Defise J.M., Delaboudinière J.P., Catura R.C. , Clette F., Maucherat A.J., "Calibration of the EIT Instrument", SPIE **2517**, 29-39, 1995.
3. Moses D.J., SOHO Intercalibration Conference, Berlin, Nov 1996.
4. Defise J.M., Clette F., Moses J.D., Hochedez J.F. and the EIT Consortium, "In-orbit diagnostic of the EIT EUV CCD radiation induced aging.", SPIE **3114**, 598-607, 1997.
5. Moses et al, "EIT Observations of the Extreme Ultraviolet Sun", Solar Physics **175,** 571-599, 1997.
6. Jannesick J.R., Klaasen K.P., Eliott T., Optical Engineering, **26**, N°10, Oct 1987
7. Robinson L.B., "A review of surface treatment for CCD's", ESO/OHP Workshop on the Optimization of the Use of CCD Detectors in Astronomy, 1986.
8. Moses D.J., "EIT Calroc initial results", SOHO Intercalibration Conference, Orsay, Nov 1997.